

Fluorescence Enhancement of Unconstrained GFP Chromophore Analogues Based on the Push–Pull Substituent Effect

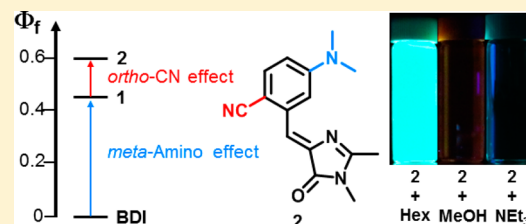
Meng-Shiue Tsai,^{†,‡} Chun-Lin Ou,[†] Chi-Jui Tsai,[†] Yen-Chin Huang,[†] Yuan-Chung Cheng,^{*,†} Shih-Sheng Sun,^{*,‡} and Jye-Shane Yang^{*,†}

[†]Department of Chemistry, National Taiwan University, Taipei 10617, Taiwan

[‡]Institute of Chemistry, Academia Sinica, Taipei 11529, Taiwan

S Supporting Information

ABSTRACT: Unlike the high fluorescence quantum yield of the naturally occurring green fluorescence protein (GFP, $\Phi_f \sim 0.8$), the GFP chromophore, a benzylidenedimethylimidazolinone (BDI) dye, is nearly nonfluorescent ($\Phi_f < 0.001$) in common solutions at room temperature. While many efforts have been devoted into the BDI chromophore engineering for fluorescence recovery, limited success has been achieved for structurally unconstrained GFP chromophore analogues (uGFPc). Herein we report a rational design of uGFPc toward an unprecedentedly high fluorescence quantum efficiency of 0.60 in hexane. This is achieved by a combined *ortho*-CN and *meta*-dimethylamino substituent electronic effect that largely suppresses the *Z* \rightarrow *E* photoisomerization (the τ torsion) reaction, which is the major nonradiative decay channel of uGFPc. The structural design relied on the assumptions that the τ torsion of the *meta*-amino-substituted BDI systems leads to a zwitterionic twisted intermediate state (${}^1P^*$) and that destabilizing the ${}^1P^*$ state by an electron-withdrawing CN substituent at the *ortho* or *para* position could slow down the τ torsion. The observed CN position effect conforms to the design concept. The push–pull substitution of BDI also leads to sensitive fluorescence-quenching responses to electron donors such as trimethylamine and to H-bond donors such as methanol.

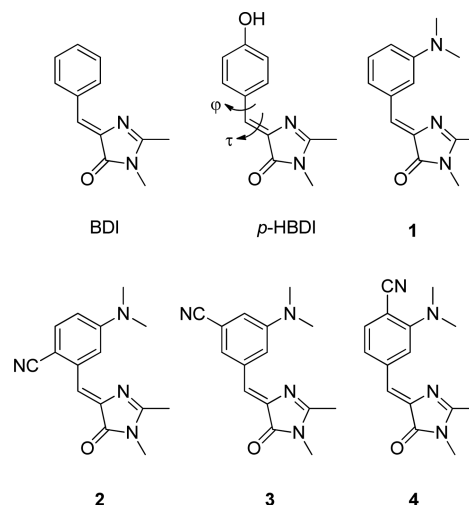


INTRODUCTION

A practical approach toward the development of highly fluorescent organic dyes for biological and materials science applications is through substituent engineering of a known chromophore.^{1–5} The substituent effect could modify the radiative vs nonradiative decay rate of the excited system by electronic or steric perturbations for fluorescence enhancement. However, to construct a simple model that correlates the nature and position of substituents with the excited-state kinetics for a rational structural design of a highly fluorescent dye is by no means trivial, particularly for those based on electronic modifications. Herein we report one such example with the benzylidenedimethylimidazolinone (BDI) chromophore (Chart 1), which is well-known by the *p*-hydroxy-substituted derivative *p*-HBDI of the green fluorescence protein (GFP) chromophore.^{6,7}

The distinct fluorescence quantum efficiency between the naturally occurring protein GFP ($\Phi_f \sim 0.8$)⁸ and its chromophore *p*-HBDI ($\Phi_f < 0.001$)⁹ in solutions at ambient temperature has attracted numerous studies toward understanding the fluorescence-quenching mechanism and in chromophore engineering for fluorescence recovery.^{10–25} It is currently known that an ultrafast torsional motion about the exocyclic C=C (the τ torsion) or C–C bond (the ϕ torsion) is responsible for the fluorescence quenching of *p*-HBDI, and an environmental constraint of these torsions imposed by the barrel-shaped protein matrix accounts for the strong fluorescence

Chart 1. Structures of BDI Chromophore and Its Derivatives



of GFP.^{10–15} Therefore, substantial fluorescence recovery has been achieved for structurally constrained analogues of *p*-HBDI created by covalent or noncovalent bridging of the two rings, which simultaneously inhibits the τ and ϕ torsions.^{16–19} Besides

Received: May 23, 2017

Published: July 20, 2017

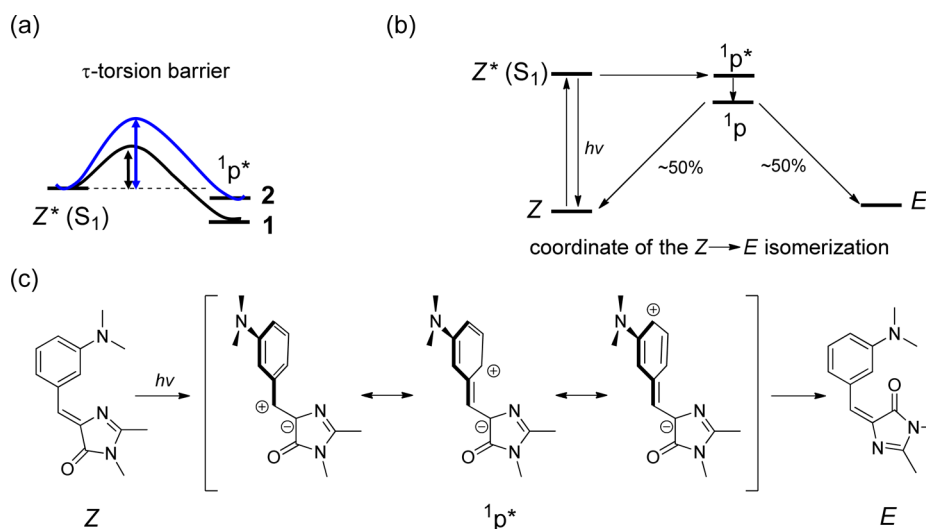


Figure 1. Concept of our rational chromophore design for fluorescence enhancement by slowing down the τ -torsion (the $Z^* \rightarrow {}^1p^*$ reaction) in S_1 : (a) An increase of the τ -torsion barrier predicted for **2** vs **1** as a result of CN-induced destabilization of the ${}^1p^*$ state. (b) The one-bond-flip mechanism for the $Z \rightarrow E$ photoisomerization of BDI systems. (c) The resonance structures of a proposed zwitterionic ${}^1p^*$ intermediate during the $Z \rightarrow E$ photoisomerization of **1**.

the conformational lock by substituents, the alternative strategy of raising the inherent torsional barriers by the substituent electronic effects (i.e., a kinetic confinement) for the structurally unconstrained counterparts has been shown to be viable.^{20–25} One particular example is the *meta*-amino derivative **1** (Chart 1),²² which displays an unprecedentedly high Φ_f value of 0.46 for structurally unconstrained GFP chromophore analogues (uGFPc).^{20–25} The *meta*-amino effect also results in high solvatofluorochromicity in aprotic solvents and H-bond-mediated fluorescence quenching activity in protic solvents.^{22,26,27} While the fluorescence features of **1** hold great promise for real-time fluorescence imaging of biological systems,²⁸ chromophores of improved fluorescence quantum efficiency are desirable. This raises the fundamental question as to how high the Φ_f of a uGFPc can be achieved with the kinetic confinement. In this context, we have carried out a rational design based on the decay mechanism of **1**. The resulting derivative **2** sets a new Φ_f record of 0.60 for uGFPc and displays a fluorescence-quenching response to electron donors that was not observed for **1**. The positional isomers **3** and **4** were also prepared to further support the mechanistic model of fluorescence enhancement.

RESULTS AND DISCUSSION

Molecular Design. A rational modification of **1** to further enhance the fluorescence quantum efficiency of uGFPc is the main goal of this work. The design concept relies on the fact that the τ torsion (i.e., the $Z^* \rightarrow {}^1p^*$ reaction in the $Z \rightarrow E$ photoisomerization coordinate of the one-bond-flip mechanism,²⁹ Figures 1a and 1b) is the main nonradiative decay channel for **1** in aprotic solvents.²² The τ torsion for **1** in the lowest singlet excited (S_1) state is likely to produce a perpendicular intermediate (${}^1p^*$) of a zwitterionic character due to the aniline-to-imidazolinone charge-transfer character, and the decoupled positive and negative charges are expected to locate at the donor and acceptor moiety, respectively, for better stabilization (Figure 1c). According to the concept of the Hammond postulate, destabilizing the reactive intermediate for a reaction could raise the reaction barrier and decrease the reaction rate.³⁰ We thus proposed that the ${}^1p^*$ state might be destabilized

to raise the τ -torsion barrier further in favor of the fluorescence emission by adding an electron-withdrawing group to the positions that bear a positive charge in the resonance structures. In this context, the strong electron-withdrawing and linear-shaped CN group was selected, and for the synthetic feasibility the CN substituent was designed to locate on the aniline moiety rather than on the exocyclic carbon. Although both the ortho and para positions of the phenylene ring bear the positive charge in resonance, the latter might encounter certain degree of steric interactions between the CN and dimethylamino (DMA) groups, which could attenuate the fluorescence-enhancing *meta*-amino effect.²⁰ Therefore, it is anticipated that the ${}^1p^*$ vs Z^* state for **2** is destabilized relative to that for **1** and the situation for **4** would depend on the extent of steric interactions; in contrast, the CN effect on the relative energy of Z^* and ${}^1p^*$ state would be relatively small for the *meta* system **3**. Consequently, the energy barrier for the τ -torsion and thus the fluorescence quantum yield would be increased for **2** relative to **1**. To gain a full picture on the CN position effect, all three systems **2–4** have been prepared for investigation.

The hypothesis of CN-induced destabilization of the ${}^1p^*$ state relative to the Z^* state for **1** has been examined by time-dependent density function theory (TDDFT) calculations at the level of M06-2X/6-31+G(d). The calculation details are provided in the Experimental Section. Figure 2 shows the relative energies of the Z^* (the reference state), ${}^1p^*$, and E^* excited states of BDI as well as **1–4**. While the E^* vs Z^* state energy is weakly perturbed by the CN substitution, the ${}^1p^*$ state energy is sensitive to the position of the CN substituent. The size

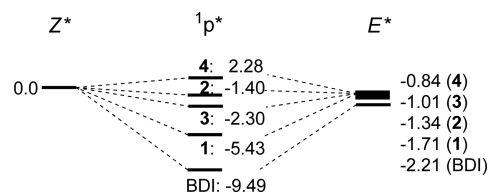
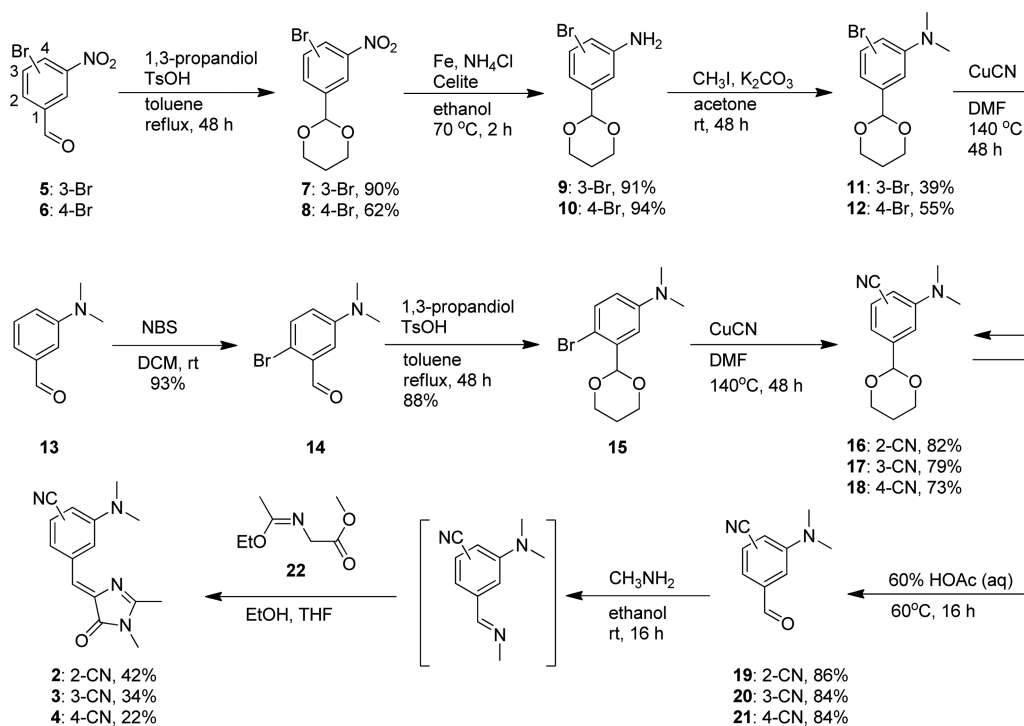


Figure 2. TDDFT-derived relative energies (kcal mol⁻¹) of the Z^* (the reference state), ${}^1p^*$, and E^* states of BDI and **1–4**.

Scheme 1. Synthesis of uGFPc 2–4



of CN-induced destabilization of $^1p^*$ is in the order 4 (7.71 kcal mol⁻¹) > 2 (4.03 kcal mol⁻¹) > 3 (3.13 kcal mol⁻¹), which is qualitatively consistent with the picture of charge resonance in Figure 1c, where the destabilization is expected to be larger for the ortho and para substitution than the meta substitution. For comparison, the fluorescence-enhancing *meta*-amino effect of **1** vs BDI was calculated to be a consequence of the $^1p^*$ destabilization (or alternatively the Z^* stabilization) by 4.06 kcal mol⁻¹. Although the relative size of energy difference between the Z^* and $^1p^*$ states might not truly reflect the relative τ -torsion barriers of **1–4** and BDI and thus the observed experimental data (vide infra), the TDDFT calculations have provided a theoretical support of our structure design toward fluorescence enhancement of uGFPc.

Synthesis and Structure. The synthesis of compounds **2–4** is shown in Scheme 1. The construction of the BDI chromophore adopted the protocol of Bazureau and Kowalik:³¹ [2 + 3] cyclocondensation of the corresponding arylideneimines with the imidate ylide methyl 2-(1-ethoxyethylideneamino)acetate (**22**). The arylideneimines were in turn prepared by reacting the precursors **19–21** with 2 equiv of methylamine in ethanol at room temperature for 16 h, and the crude liquid products after solvent removal were directly subjected to the [3 + 2] cyclocondensation reactions. The synthesis of **19–21** started from 3-bromo-*N,N*-dimethylaniline (**13**), 3-bromo-5-nitrobenzaldehyde (**5**), and 4-bromo-3-nitrobenzaldehyde (**6**), respectively, through a series of functional group transformation reactions, including protection and later deprotection of the formyl group, reduction and subsequent *N*-methylation of the nitro group, and bromination and cyanization on the phenylene ring. Details of the synthetic procedures and structural characterization data for **2–4** and intermediate compounds **7–12** and **14–21** are shown in the Experimental Section.

The X-ray crystal structures of **2** and **3** reveal a nearly planar geometry of the chromophores (Figure 3), which resembles the case of **1**.²² Table 1 summarizes the dihedral angle (α) of the two

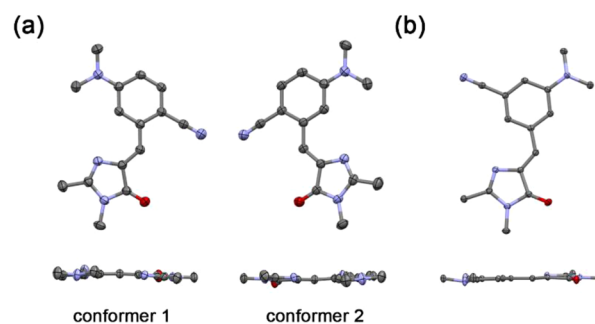


Figure 3. X-ray crystal structures (front and side views) of (a) **2** and (b) **3** in 50% probability of thermal ellipsoids. Hydrogen atoms are omitted for clarity.

Table 1. Selected Structural Parameters for **1–4** in the X-ray Crystal and/or DFT-Optimized Structures

compd	X-ray crystal			DFT-optimized		
	α^a	β^b	χ^c	α^a	β^b	χ^c
1	2.8°	6.7°	359.7°	0.4°	1.1°	353.8°
2	7.8°	0.5°	359.8°	0.1°	0.2°	359.2°
3	6.2°	2.5°	358.1°	0.5°	0.3°	356.1°
4	4.8°	1.9°	355.2°	2.9°	38.0°	344.8°
	n.a. ^d	n.a. ^d	n.a. ^d			

^a α = dihedral angle of the two rings. ^b β = the averaged phenylene-amino C–N torsion angle. ^c χ = sum of bond angles about the amino N atom. ^dn.a. = not available.

rings, the phenylene-amino C–N torsion angle (β), and the sum of bond angles (χ) about the N atom of the DMA group. For comparison, the corresponding X-ray structural data for **1** are also included. Note that the crystal of **2** consists of two structurally independent conformers, which differ slightly in the molecular planarity. It is also noted that the DMA group is in a

syn orientation to the carbonyl group in **1** and **3**, but it is anti in **2**. Regarding the CN group, it is parallel to the carbonyl group in both **2** (syn-parallel) and **3** (antiparallel).

To gain structural information about **4**, the corresponding DFT (M06-2X/6-31+G(d))-optimized structural data of α , β , and γ for **1–4** are also listed in Table 1. The calculations confirm a planar structure for **1–3** but there is a twist of 38° for the DMA group from the BDI π -moiety in **4** as a result of the steric interactions with the neighboring CN group (Figure S1). The twist is accompanied by a pyramidalization of the amino N atom, as indicated by the decreased γ value from 354 to 359° in **1–3** to 345° in **4**, which reflects a decreased conjugation (electronic coupling) for the amino lone pair with the BDI π system.

Electronic Spectra. The absorption spectra of **1–4** in hexane are shown in Figure 4. Compared to **1**, the additional CN

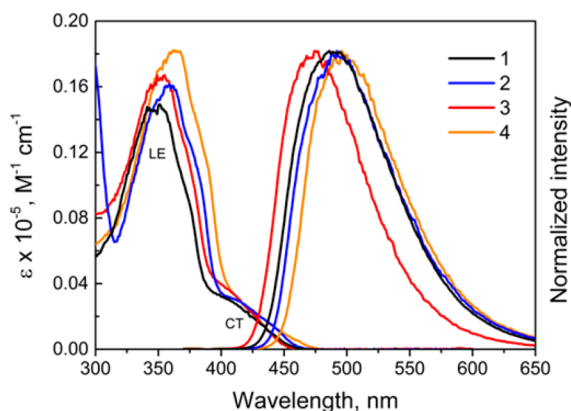


Figure 4. Absorption and fluorescence spectra of **1–4** in hexane.

group in **2–4** does not change the absorption profile, which consists of an intense BDI-based locally excited (LE) π - π^* transition band near 360 nm and a broad shoulder with absorbance up to 480 nm attributable to the aniline-to-imidazolinone charge-transfer (CT) transition.²² However, the CN substitution causes a red shift of the absorption spectra with a size depending on the CN position: namely, the wavelength of absorption maximum (λ_{abs} , nm) is in the order $4 > 2 > 3 > 1$ in both hexane and acetonitrile (Table 2). Evidently, the CN effect on λ_{abs} (from the LE band) mainly results from an elongation of

the BDI-conjugation length, which follows the general trend para > ortho > meta.

Figure 4 also shows the fluorescence spectra of **1–4** in hexane. The broad fluorescence profile for **2–4** resembles that for **1**, indicating a common CT character of the S_1 state. Indeed, a large positive solvatofluorochromism from blue to reddish orange observed for them on going from nonpolar hexane to polar DMSO (Figure 5) is consistent with a highly polar CT S_1 state.

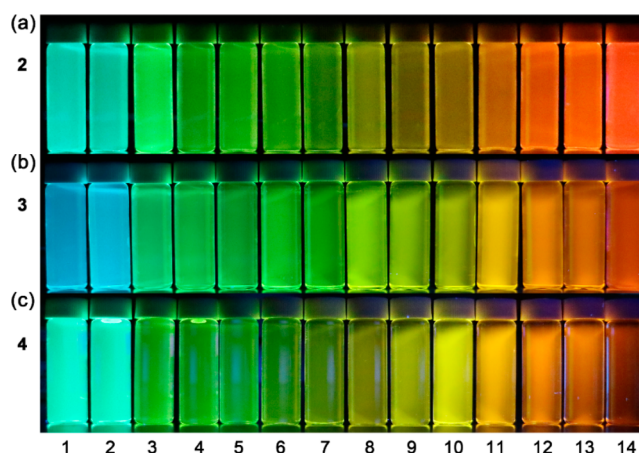


Figure 5. Photographic images for the solvatofluorochromism of (a) **2**, (b) **3**, and (c) **4** in 14 different solvents with excitation at 366 nm by a hand-held UV lamp. Solvents from left to right: (1) hexane, (2) methylcyclohexane, (3) *p*-xylene, (4) toluene, (5) diethyl ether, (6) furan, (7) chloroform, (8) tetrahydrofuran, (9) dichloromethane, (10) 1,2-dichloroethane, (11) acetone, (12) acetonitrile, (13) *N,N*-dimethylmethanamide, and (14) dimethyl sulfoxide.

The wavelength of fluorescence maximum (λ_f , nm) is in the order $4 > 2 > 1 > 3$ in hexane but becomes $1 > 2 > 3 > 4$ in acetonitrile. The hexane-to-acetonitrile solvatofluorochromic shift is in the order **1** (~ 4550 cm^{-1}) > **3** (~ 4250 cm^{-1}) > **2** (~ 3820 cm^{-1}) > **4** (~ 3370 cm^{-1}). The μ_e of the CT (Figure S2) state could be estimated by the slope (m_f) of the solvatofluorochromic plot of the energies of the fluorescence maxima against the solvent parameter Δf according to eq 1:^{32,33}

$$\nu_f = -[(1/4\pi\epsilon_0)(2/hca^3)][\mu_e(\mu_e - \mu_g)]\Delta f + \text{constant} \quad (1)$$

Table 2. Photophysical and Photochemical Data of **1–4** in Selected Solvents

compd	solvent	λ_{abs} (nm)	λ_f (nm)	Φ_f (%)	Φ_{ZE}^b (%)	τ_f^c (ns)	k_f (10^8 s^{-1})	k_{nr} (10^8 s^{-1})
1 ^a	Hex	352	486	46 ± 1	21 ± 3	22.5	0.20	0.24
	THF	354	566	14 ± 1	38 ± 4	15.3	0.09	0.56
	MeCN	354	624	5 ± 1	53 ± 5	8.6	0.06	1.11
2	Hex	359	492	60 ± 1	15 ± 3	24.7	0.24	0.16
	THF	363	560	19 ± 2	36 ± 2	14.8	0.13	0.55
	MeCN	361	606	7 ± 1	44 ± 4	7.0	0.10	1.33
3	Hex	355	475	45 ± 3	20 ± 3	21.2	0.21	0.26
	THF	359	544	14 ± 2	38 ± 2	15.1	0.09	0.57
	MeCN	354	595	5 ± 1	48 ± 5	6.0	0.08	1.58
4	Hex	362	496	41 ± 2	22 ± 2	16.0	0.27	0.37
	THF	368	568	7 ± 1	45 ± 3	6.8	0.10	1.37
	MeCN	369	592	2 ± 1	49 ± 6	3.5	0.06	2.80

^aData from ref 22. ^bExcitation wavelength is 350 nm. Solutions are at a concentration of 1×10^{-3} M. Hexane (Hex) solutions contain 30% dichloromethane (DCM) and acetonitrile (MeCN) solutions contain 20% DCM by reason for solubility. ^cDetermined with excitation at λ_{abs} and emission at λ_f .

where

$$\Delta f = (\varepsilon - 1)/(2\varepsilon + 1) - 0.5(n^2 - 1)/(2n^2 + 1) \quad (2)$$

and

$$a = (3M/4N\pi d)^{1/3} \quad (3)$$

where ν_f is the fluorescence maximum, μ_g is the ground-state dipole moment, a is the solvent cavity (Onsager) radius, which was derived from the Avogadro number (N), molecular weight (M), and density (d), and ε , ε_0 , and n are the solvent dielectric constant, the vacuum permittivity and the solvent refractive index, respectively. The value of μ_g was calculated using the DFT (M06-2X/6-31+G(d)) algorithm. The data of a , m_f , μ_g , and μ_e for 1–4 are summarized in Table 3. The μ_g and μ_e values of 2 (9.8

Table 3. Ground- and Excited-State Dipole Moments for 1–4

compd	a (Å) ^a	m_f (cm ⁻¹) ^b	μ_g (D) ^c	μ_e (D) ^b
1	4.59	12219	4.5	13.3 ± 0.9
2	4.74	10251	9.8	16.4 ± 0.8
3	4.74	11667	9.4	16.7 ± 0.8
4	4.74	8925	7.4	14.1 ± 0.7

^aOnsager radius from eq 3 with $d = 1.0 \text{ g cm}^{-3}$ for all cases. ^bCalculated on the basis of eq 1. ^cCalculated by DFT (M06-2X/6-31+G(d)).

and 16.4 D) and 3 (9.4 and 16.7 D) are relatively larger than those of 1 (4.5 and 13.3 D) and 4 (7.4 and 14.1 D). Evidently, the *ortho*- and *meta*-CN substitutions impose a larger effect than the *para*-CN substitution on the molecular polarity in both the S_0 and S_1 states.

The donor moiety of 4-(*N,N*-dimethylamino)benzonitrile (DMABN) in 2 raises a concern about its potential influence in the fluorescence of 2. DMABN is a well-documented dual emissive chromophore, and the short- and long-wavelength emission bands correspond to a LE and a twisted intramolecular charge-transfer (TICT) state, respectively.³⁴ For example, in acetonitrile the LE band is located at 353 nm and the TICT band at 469 nm. On the basis of the lack of dual emission for 2 and the similar photophysical properties among 1–4, including the absorption profiles, the fluorescence properties, and the BDI-based HOMO and LUMO (Figure S3), we conclude that the observed fluorescence for 2 results from a 1-like CT state rather than a DMABN-like TICT state. A lower state energy for the former than the latter state is responsible for the silence of the DMABN character in the S_1 state of 2.

Quantum Yields and Lifetimes. The fluorescence quantum yields (Φ_f) for 1–4 in hexane, THF, and acetonitrile are listed in Table 2. Like the case of 1,²² the Φ_f for 2–4 is high in hexane and decreases as the solvent polarity is increased. In hexane the Φ_f is in the order 2 (0.60 ± 0.01) > 1 (0.46 ± 0.01) ≈ 3 (0.45 ± 0.03) ≈ 4 (0.41 ± 0.02). The fluorescence enhancement for 2 vs 1 or 3 conforms to the design concepts of a destabilization of $^1p^*$ by an electron-withdrawing CN group at the *ortho* position (Figure 1). However, the size of fluorescence enhancement on going from 1 to 2 (the *ortho*-CN effect) is much less than that from BDI ($\Phi_f = 0.0014$ in benzene)³⁵ to 1 (the *meta*-DMA effect), although the TDDFT-predicted $^1p^*$ destabilization energy is similar (~4 kcal mol⁻¹) for both effects (Figure 2). This manifests that the substituent electronic effect on the τ torsion of the BDI chromophores is more complicated than the relative energies of the Z^* and $^1p^*$ states. Along the same lines, the lack of fluorescence enhance-

ment for 4 vs 1, which is apparently deviated from the prediction of the TDDFT calculations (Figure 2), might be attributed to the steric interactions between the DMA and the neighboring CN group (Table 1). Regarding the much more powerful *meta*-DMA vs *ortho*-CN effect on fluorescence enhancement, it is not unexpected that a minor steric perturbation on the *meta*-DMA effect could readily offset the expected *para*-CN effect on the τ -torsion barrier and thus the fluorescence enhancement for 4. To the best of our knowledge, the Φ_f value of 0.60 for 2 in hexane reaches the highest record to date for uGFPc in nonviscous solvents at room temperature. Interestingly, this value is the same as the Φ_f of EGFP, an engineered GFP mutant for use in mammalian cells.^{36,37}

The rationale of fluorescence enhancement for 2 vs 1 in hexane is further supported by their $Z \rightarrow E$ photoisomerization quantum yields (Φ_{ZE} , Table 2). According to the one-bond-flip mechanism for $Z \rightarrow E$ photoisomerization,^{22,29} the probability of forming E and Z -isomers from the $^1p^*$ state is similar (i.e., 50% for each, Figure 1b), and thus the quantum yield for the τ -torsion reaction could be estimated as $2\Phi_{ZE}$. The observation of $\Phi_f + 2\Phi_{ZE} \approx 1.0$ for 1–4 indicates that at ambient temperature all four systems have the common excited-state deactivation channels, that is, fluorescence and the τ -torsion reaction, and there is no new decay channel induced by the additional CN group in 2–4. With the τ torsion as the major nonradiative decay pathway, suppression of the τ -torsion reaction by increasing the torsion barrier is thus a useful approach toward fluorescence enhancement, which is consistent with the increased Φ_f at the expense of Φ_{ZE} for 2 in hexane.

The fluorescence lifetime (τ_f) and rate constants for the radiative ($k_f = \Phi_f / \tau_f$) and nonradiative ($k_{nr} = (1 - \Phi_f) / \tau_f$) processes provide further insights into the origin of the interplay of Φ_f and Φ_{ZE} . As shown in Table 2, the large τ_f (~20 ns) and low k_f (~2 × 10⁷ s⁻¹) values in hexane for all four systems reflect a modestly allowed optical transition for the CT (Z^*) state, consistent with the lower molar absorptivity for the CT vs the LE absorption band (Figure 4). However, it is noted that 4 possesses a somewhat larger k_f value of 2.7 × 10⁷ s⁻¹ than 1–3 (2.0–2.4 × 10⁷ s⁻¹). This might be attributed to an increase of intensity borrowing from the CT from the LE state, because the LE band of 4 is the most red-shifted such that the overlap with the CT transition is the largest among 1–4. However, the k_{nr} values are also increased for 4 as a result of the diminished *meta*-DMA effect, which ranks 4 the lowest Φ_f among 1–4 not only in hexane but also in the more polar solvents. Evidently, the planarity of the DMA group and the LE-CT energy gap are critical in determining the fluorescence quantum efficiency of 1 and its derivatives.

The phenomenon of large dependence of Φ_f and Φ_{ZE} on the solvent polarity is common for 1–4, which could be explained by the solvent-dependent *meta*-amino effect. It is known that the donor–acceptor twisted geometry of a TICT state is better stabilized in more polar solvents.^{33,34} Although there is no direct evidence of forming a DMA-twisted TICT state for 1–4 in polar solvents, the solvent polarity might affect the torsion dynamics of the DMA group in S_1 in a way that the DMA-BDI coupling is weaker in more polar solvents. Consequently, the fluorescence-enhancing *meta*-DMA effect is largely reduced in polar solvents, corresponding to a decrease of Φ_f but an increase of Φ_{ZE} . Nevertheless, the *ortho*-CN electronic effect is still noticeable in THF and MeCN, which displays an extent of fluorescence enhancement (~30%) similar to that in hexane for 2 vs 1. The larger solvent polarity effect on Φ_f for 4 vs 1–3 could be again

attributed to the pretwist of the DMA group in the ground state that facilitates the decoupling of the DMA and BDI groups in polar solvents.

Fluorescence Quenching. The feature of H-bond-induced fluorescence quenching for **1** in protic solvents such as methanol ($\Phi_f < 0.001$) is retained for **2–4** (Figure S4). Titration of the acetonitrile solution of **2–4** with methanol (Figure S5) shows a Stern–Volmer constant (K_{SV}) of 0.98–1.83 M⁻¹, which is somewhat lower than that of **1** (3.35 M⁻¹) according to the Stern–Volmer plots of $(I_0/I - 1)$ against the concentration of methanol according to eq 4:

$$I_0/I = 1 + K_{SV}[Q] \quad (4)$$

where I_0 and I are the fluorescence intensity in the absence and presence of quencher (Q). Our previous work on **1** and its derivatives showed that H-bonding of solvent molecules (H-bond donor) to the carbonyl group (H-bond acceptor) dominates the fluorescence quenching of the *meta*-amino-substituted BDI systems in protic solvents.^{22,26,27} Therefore, the lower fluorescence quenching efficiency for **2–4** by methanol could be attributed to a reduced H-bonding interactions with the carbonyl oxygen as a result of the electron-withdrawing CN substitution. Figure 6a demonstrates the fluorescence on–off–

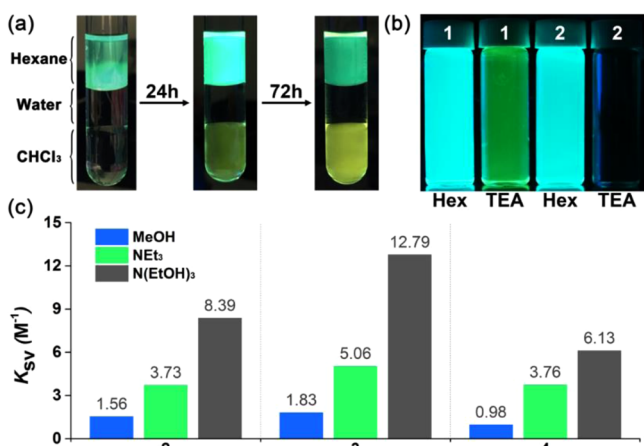


Figure 6. (a) The fluorescence on–off–on switching of **2** upon diffusion from the top hexane layer through the middle water layer to the chloroform bottom layer; (b) comparison of fluorescence responses of **2** vs **1** to NEt₃ (TEA); (c) comparison of the Stern–Volmer constants (K_{SV}) of **2–4** with the quenchers MeOH, NEt₃, and N(EtOH)₃.

on switching upon diffusion of **2** from hexane (top layer) through water (middle layer) to chloroform (bottom layer): namely, the cyan fluorescence in hexane (aprotic) is first quenched when the dye enters to the water (protic) layer and then the fluorescence is turned back on with yellow color when it reaches the chloroform (aprotic) layer. Such a fluorescence turn-on behavior might render **1–4** useful fluorescence turn-on probes for real-time imaging of the hydrophobic regions of a biological system.

A new feature observed for **2–4** relative to **1** is the fluorescence quenching in response to triethylamine (TEA, Figure 6b and Figure S4). Trialkylamines often function as electron donors that quench the fluorescence of aromatic systems through the nonradiative processes of photoinduced electron transfer (PET) or induce a long-wavelength emission band of exciplexes.³⁸ Evidently, the electron-withdrawing CN group activates the PET processes by increasing the electron-accepting ability of the electronically excited chromophores. Indeed, the

HOMO energy of **2–4** are lower than that of **1** (Figure S3), which facilitates the electron transfer from TEA to the excited state of **2–4**. The titration experiments in acetonitrile (Figure S6) show that the fluorescence quenching by TEA is 2.4–3.8 times larger than that by methanol ($K_{SV} = 3.73–5.06$ vs $0.98–1.83$ M⁻¹, Figure 6c).

Knowing that **2–4** display fluorescence-quenching responses to both H-bond and electron donors, it is interesting to compare the quenching behavior of quenchers having both the H-bond and electron donating ability with those having either one of the two characters. In this context, triethanolamine, a potential ecotoxic component present in many detergents, paints, cosmetics, and medicine,³⁹ was tested (Figure S7). The results show that the fluorescence quenching effect is additive: namely, the Stern–Volmer constant for triethanolamine is approximately equal to the sum of those for TEA and methanol of the same concentration (Figure 6c), regarding that 1 equiv of triethanolamine contains 1 equiv of TEA and 3 equiv of methanol.

CONCLUSION

A rational design of a push (amino)-pull (cyano) substituent electronic effect on driving the BDI chromophore toward fluorescence enhancement is demonstrated. Our results also show the importance of the planarity of the *meta*-amino group with the BDI π -system in determining the fluorescence quantum efficiencies. The resulting system **2** of combined *meta*-amino and *ortho*-CN substitution displays a new record of fluorescence quantum yield of 0.60 for structurally unconstrained GFP chromophore analogues in nonpolar solvents at ambient temperature. While the *meta*-amino substitution alone induces an intriguing fluorescence-quenching response to H-bond donors,²² the additional CN substitution induces a new fluorescence-quenching response to electron donors. These features might find particular utility in fluorescence sensing and imaging applications.

EXPERIMENTAL SECTION

General Methods. ¹H and ¹³C NMR spectra were recorded by using a 400 or 500 MHz spectrometer. High-resolution mass spectra were recorded for samples ionized by the methods of EI, ESI, or FAB and analyzed by the MS or TOF method. Absorption spectra were measured with a UV–vis spectrophotometer at 1 nm resolution. Fluorescence spectra were recorded with correction for the response of the detector. Fluorescence quantum yields were measured by using quinine sulfate in 0.05 M H₂SO₄ (0.52) as a standard reference.⁴⁰ The standard and substrate solutions were N₂-bubbled before the measurements and the solvent refractive index was corrected. The error for the reported Φ_f values is within $\pm 3\%$. The time-resolved fluorescence decay measurements were carried out with a spectrophotometer using a gated hydrogen arc lamp as the light source. The goodness of the nonlinear least-squares fit was judged by the reduced χ^2 value (< 1.1 in all cases), the randomness of the residuals, and the autocorrelation function. Quantum yield of photoisomerization were determined with optically dense degassed solutions ($\sim 1 \times 10^{-3}$ M) under 350 nm light irradiation of a 75-W Xe arc lamp equipped with a monochromator. The reference standard was *trans*-4-(*N*-phenylamino)stilbene ($\Phi_{ic} = 0.34$ in CH₂Cl₂).⁴¹ The extent of photoisomerization (less than 10%) was determined by HPLC without back reaction correction. The *Z* \rightarrow *E* isomerization quantum yield (Φ_{ZE}) was calculated according to eq 5:

$$\frac{C_1 \times V_1 \times P_1}{\Phi_{ZE} \times t_1} = \frac{C_2 \times V_2 \times P_2}{\Phi_{ic} \times t_2} \quad (5)$$

where the subscripts 1 and 2 denote the concentration of sample and standard, respectively; C is the concentration; V is the volume; P is the amount (%) of *trans* \rightarrow *cis* or *Z* \rightarrow *E* conversion; t is the irradiation time;

Φ_{ic} is the isomerization quantum yield of the standard. The error for the reported Φ_{ZE} values is within $\pm 6\%$. All the photophysical data were collected at 25 ± 1 °C. The Single crystal data were collected with a CCD diffractometer with Mo K α radiation.

DFT Calculations. All calculations were performed by using density functional theory (DFT) with the Gaussian 09 quantum chemistry program.⁴² The M06-2X functional developed by Zhou and Truhlar⁴³ was used in this study because of its superior performance in excited-state calculations, especially for charge transfer excitations.⁴⁴ For a balanced computational cost and accuracy, a 6-31+G(d) basis set was employed in all the calculations. Ground-state DFT geometry optimizations were used to obtain the structures of 1–4, and the frequencies were evaluated for the optimized geometries at the same level to ensure that the structure obtained was a minimum on the potential energy surface. TDDFT was employed to excited-state calculations. Excited-state geometry optimizations were performed to obtain the structures of the Z^* , 1^*p , and E^* states, respectively, and the outputs were double-checked to make sure that all the standard convergence criteria were met for the optimized structures. Note that for the 1^*p states, unrestricted TDDFT calculations were carried out to accommodate the likelihood of diradical or broken-symmetry excited states; nevertheless, in all our calculations at the 1^*p state structures, the final electronic structures of the S_1 states converged into closed-shell wave functions, confirming our assignment of the 1^*p state. We also checked the spin-density distributions on the low-lying excited states ($S_1 - S_3$) at the 1^*p structures to confirm that a diradical state is not available to alter the mechanism of radiationless decay in 1–4. We have also carried out the calculations using the Becke's three-parameter hybrid exchange functional and the Lee–Yang–Parr correlation functional (B3LYP),^{45,46} and the results were not qualitatively different and thereby not shown in this work.

Materials. All the solvents for spectra and quantum yield measurements were HPLC grade and used as received. Anhydrous THF, toluene, and DMF were obtained by standard procedures. All the other solvents and materials for synthesis were reagent grade. The synthesis of 1,²² 5,⁴⁷ 6,⁴⁸ 13,²² and 22³¹ have been reported. All the reactions were monitored by using precoated TLC plates. Purifications with column chromatography was performed on silica gel (60–120 mesh). All the new compounds were identified by 1H and ^{13}C NMR, high-resolution Mass, and IR spectroscopies.

Synthesis of 2–4. The common synthetic procedures are illustrated by the case of 2: The mixture of arylideneimine precursor 19 (1.00 g, 5.7 mmol) and 40 wt % methylamine in ethanol (0.90 mL) was stirred for 16 h at room temperature. The solvent was then removed in vacuo to afford yellow liquid crude arylideneimine product. The crude product was combined with the freshly prepared imidate ylide 22 (1.00 g, 6.3 mmol) in absolute EtOH (5.0 mL) and THF (5.0 mL), and then stirred for 24 h at room temperature. The solvent was removed under reduced pressure, and the residue was dissolved in CH₂Cl₂ and washed with brine and water. The organic layer was dried over anhydrous MgSO₄ and the filtrate was concentrated under reduced pressure. The crude product was purified by column chromatography using the eluent EA/DCM/Hex = 1/4/5 to afford 2 (yellow solid, 0.65 g, 42%): mp 199–201 °C; 1H NMR (400 MHz, CDCl₃) 8.23 (d, $J = 2.7$ Hz, 1H), 7.49 (d, $J = 8.8$ Hz, 1H), 7.37 (s, 1H), 6.64 (dd, $J = 8.8$ Hz and $J = 2.7$ Hz, 1H), 3.19 (s, 3H), 3.08 (s, 6H), 2.37 (s, 3H) ppm; $^{13}C\{^1H\}$ NMR (100 MHz, CDCl₃) 170.1, 164.5, 152.3, 140.7, 137.3, 134.2, 122.5, 119.1, 114.9, 112.4, 99.9, 39.9, 26.6, 15.9 ppm; IR (KBr) 1356, 1595, 1647, 1715, 2207, 2921 cm⁻¹; HRMS (ESI-TOF) calcd. for C₁₅H₁₇N₄O [M + H]⁺: 269.1402, found 269.1397. Product 3 (yellow solid, 0.52 g, 36%) was obtained with 20 (0.92 g, 5.3 mmol), 33 wt % methylamine in ethanol (0.98 mL), and 22 (0.92 g, 5.8 mmol) and the eluent CHCl₃/EA = 2/1: decomposed at 258 °C; 1H NMR (500 MHz, CD₂Cl₂): 7.90 (s, 1H), 7.60 (s, 1H), 6.90 (s, 1H), 6.89 (s, 1H), 3.14 (s, 3H), 3.01 (s, 6H), 2.37 (s, 3H) ppm; $^{13}C\{^1H\}$ NMR (125 MHz, CD₂Cl₂): 170.9, 161.9, 151.0, 140.8, 136.4, 125.0, 123.0, 120.0, 120.0, 116.0, 113.7, 40.5, 27.0, 16.2 ppm; IR (KBr) 3087, 2922, 2857, 2811, 2225, 1709, 1649, 1593, 1443, 1379, 1130 cm⁻¹; HRMS (FAB-MS) calcd. for C₁₅H₁₇N₄O [M + H]⁺: 269.1402, found 269.1406. Product 4 (yellow solid, 0.34 g, 22%) was obtained with 21 (1.00 g, 5.7 mmol), 33 wt % methylamine in ethanol (1.42 mL), and 22

(1.01 g, 6.3 mmol) and the eluent EA/DCM/Hex = 3/3/4: mp 178–180 °C; 1H NMR (500 MHz, CDCl₃) 7.67 (d, $J = 1.3$ Hz, 1H), 7.62 (dd, $J = 8.1$ Hz and $J = 1.3$ Hz, 1H), 7.52 (d, $J = 8.1$ Hz, 1H), 6.97 (s, 1H), 6.96 (s, 1H), 3.19 (s, 3H), 3.09 (s, 6H), 2.39 (s, 3H) ppm; $^{13}C\{^1H\}$ NMR (125 MHz, CDCl₃) 170.7, 164.5, 155.3, 140.8, 139.1, 135.2, 125.5, 122.5, 120.2, 119.8, 101.8, 43.2, 26.9, 16.1 ppm; IR (KBr) 2948, 2881, 2847, 2801, 2210, 1713, 1645, 1598, 1563, 1417, 1397, 1132, 570 cm⁻¹; HRMS (EI-MS) calcd. for C₁₅H₁₆N₄O [M]⁺: 268.1324, found 268.1327.

Synthesis of 7 and 8. The common synthetic procedures are illustrated by the case of 7: A mixture of 5 (10.00 g, 43.9 mmol), 1,3-propanediol (16.04 g, 219.3 mmol), and *p*-toluenesulfonic acid (0.83 g, 4.4 mmol) in toluene (80 mL) was heated under reflux for 48 h. The solvent was removed under reduced pressure, and the residue was dissolved in CH₂Cl₂ and washed with brine. The organic layers were dried over MgSO₄, filtered, and concentrated. The purification was carried out by column chromatography using the eluent Hex/EA = 15/1 to afford 7 (white solid, 11.34 g, 90%): mp 54–55 °C; 1H NMR (400 MHz, CDCl₃) 8.33 (s, 1H), 8.29 (s, 1H), 7.97 (s, 1H), 5.53 (s, 1H), 4.31–4.27 (m, 2H), 4.04–3.97 (m, 2H), 2.27–2.17 (m, 1H), 1.52–1.47 (m, 1H) ppm; $^{13}C\{^1H\}$ NMR (100 MHz, CDCl₃) 148.9, 142.5, 135.6, 126.9, 122.8, 120.5, 99.1, 67.6, 25.7 ppm; IR (KBr) 3091, 2972, 2928, 2858, 1538, 1376, 1345, 1149, 1112, 1050, 1027, 1008, 858, 736 cm⁻¹; HRMS (FAB-MS) calcd. for C₁₀H₁₁BrNO₄ [M + H]⁺: 287.9871, found 287.9867. Product 8 (white solid, 11.82 g, 62%) was obtained with 6 (15.00 g, 65.8 mmol), 1,3-propanediol (25.02 g, 328.9 mmol), and *p*-toluenesulfonic acid (1.25 g, 6.57 mmol) and the eluent Hex/EA = 10/1: mp 71–72 °C; 1H NMR (400 MHz, CDCl₃) 7.96 (d, $J = 2.0$ Hz, 1H), 7.71 (d, $J = 8.0$ Hz, 1H), 7.51 (dd, $J = 8.0$ Hz and $J = 2.0$ Hz, 1H), 5.48 (s, 1H), 4.28–4.23 (m, 2H), 4.00–3.93 (m, 2H), 2.25–2.12 (m, 1H), 1.56–1.43 (m, 1H) ppm; $^{13}C\{^1H\}$ NMR (100 MHz, CDCl₃) 139.8, 134.8, 130.8, 123.6, 114.4, 99.0, 94.3, 67.4, 25.5 ppm; IR (KBr) 3099, 3056, 2958, 2929, 2871, 2729, 1536, 1358, 1348, 1106, 1025, 993, 834, 819 cm⁻¹; HRMS (FAB-MS) calcd. for C₁₀H₁₁BrNO₄ [M + H]⁺: 287.9871, found 287.9867.

Synthesis of 9 and 10. The common synthetic procedures are illustrated by the case of 9: A mixture of 7 (11.34 g, 39.4 mmol), iron powder (6.59 g, 118.1 mmol), ammonium chloride (1.15 g, 19.7 mmol), water (25 mL), and Celite (11 g) in ethanol (30 mL) was heated under reflux for 2 h. The mixture was diluted with EA (100 mL) and filtered through Celite. The filtrate was concentrated and then dissolved in CH₂Cl₂ and washed with brine. The organic layers were dried over MgSO₄, filtered, and concentrated. The purification was carried out by column chromatography using Hex/EA = 4/1 as the eluent to afford 9 (yellow solid, 9.23 g, 91%): mp 104–105 °C; 1H NMR (500 MHz, DMSO-*d*₆) 6.67 (s, 1H), 6.62 (s, 1H), 6.60 (s, 1H), 5.42 (s, 2H), 5.33 (s, 1H), 4.11–4.08 (m, 2H), 3.90–3.85 (m, 2H), 1.98–1.91 (m, 1H), 1.43–1.39 (m, 1H) ppm; $^{13}C\{^1H\}$ NMR (125 MHz, DMSO-*d*₆) 150.3, 141.6, 121.4, 115.6, 115.6, 110.6, 99.9, 66.5, 25.3 ppm; IR (KBr) 3404, 3308, 3202, 2967, 2929, 2861, 1605, 1578, 1456, 1396, 1145, 1102, 1000, 990, 823 cm⁻¹; HRMS (FAB-MS) calcd. for C₁₀H₁₃BrNO₂ [M + H]⁺: 258.0130, found 258.0135. Product 10 (yellow liquid, 8.44 g, 94%) was obtained with 8 (10.00 g, 34.7 mmol), iron powder (5.82 g, 104.2 mmol), ammonium chloride (0.93 g, 17.4 mmol), water (20 mL), Celite (8 g), and ethanol (40 mL) and the eluent Hex/EA = 4/1: 1H NMR (400 MHz, DMSO-*d*₆) 7.36 (d, $J = 8.4$ Hz, 1H), 6.88 (d, $J = 2.0$ Hz, 1H), 6.69 (dd, $J = 8.4$ Hz and $J = 2.0$ Hz, 1H), 5.34 (s, 1H), 5.31 (s, 2H), 4.23–4.19 (m, 2H), 3.95–3.89 (m, 2H), 1.98–1.91 (m, 1H), 1.43–1.39 (m, 1H) ppm; $^{13}C\{^1H\}$ NMR (125 MHz, DMSO-*d*₆) 150.3, 141.6, 121.4, 115.6, 115.6, 110.6, 99.9, 66.5, 25.3 ppm; HRMS (EI-MS) calcd. for C₁₀H₁₂BrNO₂ [M]⁺: 257.0051, found 257.0053.

Synthesis of 11 and 12. The common synthetic procedures are illustrated by the case of 11: A mixture of 9 (9.24 g, 35.8 mmol), iodomethane (10.67 g, 75.2 mmol), and potassium carbonate (9.99 g, 72.3 mmol) in acetone (20 mL) was stirred at room temperature for 48 h. The solvent was removed under reduced pressure, and the residue was dissolved in CH₂Cl₂ and washed with brine. The organic layers were dried over MgSO₄, filtered, and concentrated. The purification was carried out by column chromatography using Hex/EA = 6/1 as the eluent to afford 11 (yellow solid, 3.98 g, 39%): mp 84.8–85.8 °C; 1H

NMR (500 MHz, DMSO-*d*₆) 6.80 (s, 1H), 6.78 (s, 1H), 6.69 (s, 1H), 5.42 (s, 1H), 4.13–4.11 (m, 2H), 3.92–3.87 (m, 2H), 2.89 (s, 6H), 2.02–1.93 (m, 1H), 1.44–1.41 (m, 1H) ppm; ¹³C{¹H} NMR (125 MHz, DMSO-*d*₆) 151.3, 141.6, 122.1, 116.1, 114.2, 108.9, 100.2, 66.3, 40.0, 25.3 ppm; IR (KBr) 2970, 2921, 2852, 2804, 1605, 1565, 1493, 1437, 1376, 1235, 1152, 1106, 1003, 984, 828 cm⁻¹; HRMS (FAB-MS) calcd. for C₁₂H₁₆BrNO₂ [M + H]⁺: 285.0364, found 285.0357. Product **12** (yellow solid, 5.04 g, 55%) was obtained with **10** (8.33 g, 32.3 mmol), iodomethane (9.61 g, 67.7 mmol), and potassium carbonate (8.91 g, 64.4 mmol) and the eluent Hex/EA = 5/1: mp 49–50 °C; ¹H NMR (500 MHz, CDCl₃) 7.54 (d, *J* = 8.2 Hz, 1H), 7.23 (d, *J* = 2.0 Hz, 1H), 7.00 (dd, *J* = 8.2 Hz and *J* = 2.0 Hz, 1H), 5.44 (s, 1H), 4.28–4.25 (m, 2H), 4.01–3.95 (m, 2H), 2.81 (s, 6H), 2.25–2.19 (m, 1H), 1.47–1.43 (m, 1H) ppm; ¹³C{¹H} NMR (125 MHz, CDCl₃) 152.0, 139.1, 133.9, 121.9, 119.6, 118.3, 101.2, 67.6, 44.4, 25.9 ppm; IR (KBr) 2950, 2852, 2782, 1595, 1574, 1480, 1458, 1388, 1378, 1149, 1106, 1024, 1012 cm⁻¹; HRMS (EI-MS) calcd. for C₁₂H₁₆BrNO₂ [M]⁺: 285.0364, found 285.0359.

Synthesis of 14. To a solution of **13** (5.97 g, 40.0 mmol) in dichloromethane (100 mL) was added *N*-bromosuccinimide (5.87 g, 38.6 mmol) at 0 °C and then warmed to room temperature with stir for 3 h. The solvent was removed under reduced pressure, and the residue was dissolved in CH₂Cl₂ and washed with brine. The organic layers were dried over MgSO₄, filtered, and concentrated. The purification was carried out by column chromatography with Hex/DCM (5/1) as the eluent to afford yellow solid **14** (8.19 g, 90%): mp 76–77 °C; ¹H NMR (400 MHz, CDCl₃) 10.23 (s, 1H), 7.34 (d, *J* = 8.9 Hz, 1H), 7.10 (d, *J* = 3.3 Hz, 1H), 6.71 (dd, *J* = 8.9 Hz and *J* = 3.3 Hz, 1H), 2.92 (s, 6H) ppm; ¹³C{¹H} NMR (100 MHz, CDCl₃) 192.2, 149.7, 133.7, 133.0, 119.0, 112.7, 111.8, 40.1 ppm; IR (KBr) 2894, 1694, 1599, 1504, 1398, 1145, 853, 809 cm⁻¹; HRMS (ESI-TOF) calcd. for C₉H₁₁BrNO [M + H]⁺: 228.0019, found 228.0019.

Synthesis of 15. A mixture of **14** (8.19 g, 36.0 mmol), 1,3-propanediol (13.82 g, 179.6 mmol), and *p*-toluenesulfonic acid (0.62 g, 3.6 mmol) in toluene (80 mL) was heated under reflux for 48 h. The solvent was removed under reduced pressure, and the residue was dissolved in CH₂Cl₂ and washed with brine. The organic layers were dried over MgSO₄, filtered, and concentrated. The purification was carried out by column chromatography with Hex/EA = 15/1 as the eluent to afford yellow liquid **15** (9.07 g, 88%): ¹H NMR (400 MHz, CDCl₃) 7.32 (d, *J* = 8.9 Hz, 1H), 7.04 (d, *J* = 3.2 Hz, 1H), 6.56 (dd, *J* = 8.9 Hz and *J* = 3.2 Hz, 1H), 5.71 (s, 1H), 4.24–4.29 (m, 2H), 3.99–4.06 (m, 2H), 2.94 (s, 6H), 2.20–2.30 (m, 1H), 1.42–1.46 (m, 1H) ppm; ¹³C{¹H} NMR (100 MHz, CDCl₃) 150.0, 137.2, 132.6, 114.6, 111.6, 108.2, 101.2, 67.5, 40.5, 25.6 ppm; IR (KBr) 2925, 1597, 1495, 1111 cm⁻¹; HRMS (ESI-TOF) calcd. for C₁₂H₁₇BrNO₂ [M + H]⁺: 286.0437, found 286.0437.

Synthesis of 16–18. The common synthetic procedures are illustrated by the case of **16**: A mixture of **15** (9.07 g, 32.0 mmol) and copper(I) cyanide (14.19 g, 158.0 mmol) in dry DMF (55 mL) was heated to 140 °C for 48 h and then cooled down to room temperature. The solution was added with a portion of CH₂Cl₂ (30 mL) and then filtered. The filtrate was washed with brine, and the organic layers were dried over MgSO₄ and filtered. The solvent was removed in vacuo, and the purification was carried out by column chromatography using Hex/EA = 5/1 as the eluent to afford **16** (white solid, 6.10 g, 82%): mp 77–79 °C; ¹H NMR (400 MHz, CDCl₃) 7.39 (d, *J* = 8.8 Hz, 1H), 6.92 (d, *J* = 2.7 Hz, 1H), 6.54 (dd, *J* = 8.8 Hz and *J* = 2.7 Hz, 1H), 5.67 (s, 1H), 4.22–4.26 (m, 2H), 3.97–4.03 (m, 2H), 2.99 (s, 6H), 2.15–2.28 (m, 1H), 1.41–1.45 (m, 1H) ppm; ¹³C{¹H} NMR (100 MHz, CDCl₃) 152.4, 142.2, 133.8, 118.8, 111.2, 108.9, 99.5, 95.7, 67.4, 39.7, 25.3 ppm; IR (KBr) 2964, 2928, 2862, 2208, 1614, 1519, 1080 cm⁻¹; HRMS (ESI-TOF) calcd. for C₁₃H₁₇N₂O₂ [M + H]⁺: 233.1285, found 233.1285. Product **17** (white solid, 0.30 g, 79%) was obtained with **11** (0.50 g, 1.8 mmol) and CuCN (0.78 g, 8.7 mmol) in dry DMF (20 mL) and the eluent Hex/EA = 5/1: mp 102–103 °C; ¹H NMR (500 MHz, CDCl₃) 7.09 (s, 1H), 7.01 (s, 1H), 6.86 (s, 1H), 5.44 (s, 1H), 4.29–4.25 (m, 2H), 4.01–3.99 (m, 2H), 2.99 (s, 6H), 2.26–2.18 (m, 1H), 1.48–1.44 (m, 1H) ppm; ¹³C{¹H} NMR (125 MHz, CDCl₃) 150.3, 140.9, 119.7, 117.9, 115.6, 114.3, 113.0, 100.8, 67.6, 40.6, 25.8 ppm; IR (KBr) 2967,

2926, 2854, 2227, 1603, 1496, 1394, 1240, 1148, 1106, 998, 840 cm⁻¹; HRMS (FAB-MS) calcd. for C₁₃H₁₆N₂O₂ [M + H]⁺: 232.1212, found 232.1217. Product **18** (yellow solid, 1.66 g, 73%) was obtained with **12** (2.79 g, 9.73 mmol) and CuCN (4.36 g, 48.66 mmol) in dry DMF (20 mL) and the eluent Hex/EA = 6/1: mp 95–97 °C; ¹H NMR (500 MHz, CDCl₃) 7.50 (d, *J* = 8.0 Hz, 1H), 7.04 (d, *J* = 1.0 Hz, 1H), 6.95 (dd, *J* = 8.0 Hz and *J* = 1.0 Hz, 1H), 5.45 (s, 1H), 4.29–4.25 (m, 2H), 4.00–3.95 (m, 2H), 3.05 (s, 6H), 2.25–2.18 (m, 1H), 1.48–1.44 (m, 1H) ppm; ¹³C{¹H} NMR (125 MHz, CDCl₃) 155.7, 144.1, 135.2, 119.8, 117.2, 114.5, 101.6, 100.8, 67.6, 43.2, 25.9 ppm; IR (KBr) 2986, 2960, 2936, 2876, 2841, 2794, 2217, 1609, 1567, 1502, 1461, 1413, 1382, 1158, 1099, 1025, 1013, 967, 814 cm⁻¹; HRMS (EI-MS) calcd. for C₁₃H₁₆N₂O₂ [M]⁺: 232.1212, found 232.1206.

Synthesis of 19–21. The common synthetic procedures are illustrated by the case of **19**: The solution of **16** (6.10 g, 26.0 mmol) in 60% acetic acid solution (50 mL) was heated at 60 °C for 16 h. The solution was neutralized with 10% NaOH(aq) and then added with CH₂Cl₂ and washed with brine. The organic portion were dried over MgSO₄ and filtered. The solvent was removed in vacuo, and the purification was carried out by recrystallization in Hex/DCM to afford **19** (yellow solid, 3.89 g, 86%): mp 119–121 °C; ¹H NMR (400 MHz, CDCl₃) 10.24 (s, 1H), 7.56 (d, *J* = 8.8 Hz, 1H), 7.15 (d, *J* = 2.8 Hz, 1H), 6.83 (dd, *J* = 8.8 Hz and *J* = 2.8 Hz, 1H), 3.10 (s, 6H) ppm; ¹³C{¹H} NMR (100 MHz, CDCl₃) 189.6, 152.3, 137.7, 135.0, 117.7, 115.7, 111.0, 98.7, 39.9 ppm; IR (KBr) 2922, 2214, 1696, 1611, 1525 cm⁻¹; HRMS (ESI-TOF) calcd. for C₁₀H₁₀N₂NaO [M + Na]⁺: 197.0685, found 197.0678. Product **20** (yellow solid, 0.24 g, 84%) was obtained with **17** (0.35 g, 1.6 mmol) in 60% acetic acid (30 mL): mp 133–134 °C; ¹H NMR (500 MHz, CDCl₃) 9.94 (s, 1H), 7.40 (s, 1H), 7.32 (s, 1H), 7.09 (s, 1H), 3.06 (s, 6H) ppm; ¹³C{¹H} NMR (125 MHz, CDCl₃) 191.3, 150.8, 137.9, 120.8, 119.8, 118.8, 115.3, 114.1, 40.4 ppm; IR (KBr) 3075, 2921, 2869, 2816, 2741, 2230, 1697, 1599, 1501, 1378 cm⁻¹; HRMS (FAB-MS) calcd. for C₁₀H₁₀N₂O [M + H]⁺: 174.0791, found 174.0789. Product **21** (yellow solid, 1.04 g, 84%) was obtained with **18** (1.66 g, 7.1 mmol) in 60% acetic acid (30 mL): mp 62–64 °C; ¹H NMR (500 MHz, CDCl₃) 9.89 (s, 1H), 7.67 (d, *J* = 8.0 Hz, 1H), 7.34 (d, *J* = 1.0 Hz, 1H), 7.29 (dd, *J* = 8.0 Hz and *J* = 1 Hz, 1H), 3.15 (s, 6H) ppm; ¹³C{¹H} NMR (125 MHz, CDCl₃) 191.8, 155.4, 139.7, 136.3, 119.3, 119.1, 116.8, 105.1, 43.1 ppm; IR (KBr) 2953, 2852, 2809, 2732, 2214, 1702, 1603, 1557, 1503, 1453, 1419, 1387, 1297, 1201, 761 cm⁻¹; HRMS (EI-MS) calcd. for C₁₀H₁₀N₂O [M]⁺: 174.0793, found 174.0787.

■ ASSOCIATED CONTENT

📄 Supporting Information

The Supporting Information is available free of charge on the ACS Publications website at DOI: 10.1021/acs.joc.7b01260.

DFT-derived frontier molecular orbitals, molecular structures, and Cartesian coordinates, solvatofluorochromic plots, fluorescence-quenching photos and profiles, and ¹H and ¹³C NMR spectra of new compounds (PDF)

X-ray crystal structure of **2** (CIF)

X-ray crystal structure of **3** (CIF)

■ AUTHOR INFORMATION

Corresponding Authors

*E-mail: yuanchung@ntu.edu.tw.

*E-mail: sssun@chem.sinica.edu.tw.

*E-mail: jsyang@ntu.edu.tw.

ORCID

Jye-Shane Yang: 0000-0003-4022-2989

Notes

The authors declare no competing financial interest.

ACKNOWLEDGMENTS

We thank the Ministry of Science and Technology (MOST 104-2113-M-002-004-MY3 and MOST 103-2113-M-001-026-MY3) of Taiwan, Academia Sinica (AS), and National Taiwan University (NTU, 106R880201) for financial support. The computing time was provided by the Computing Center of NTU. We also thank Prof. Shie-Ming Peng and Mr. Yi-Hung Liu at NTU and Dr. Yuh-Sheng Wen at the X-ray Center of Institute of Chemistry, AS, for the X-ray crystallography of **2** and **3**, respectively. Mass spectrometry analyses were performed by Mass Spectrometry facility of the Institute of Chemistry, AS and Department of Chemistry, NTU.

REFERENCES

- (1) Liu, J.; Diwu, Z.; Leung, W.-Y.; Lu, Y.; Patch, B.; Haugland, R. P. *Tetrahedron Lett.* **2003**, *44*, 4355–4359.
- (2) Butler, R. S.; Myers, A. K.; Bellarmine, P.; Abboud, K. A.; Castellano, R. K. *J. Mater. Chem.* **2007**, *17*, 1863–1865.
- (3) Hammershøj, P.; Sørensen, T. J.; Han, B.-H.; Laursen, B. W. *J. Org. Chem.* **2012**, *77*, 5606–5612.
- (4) Niko, Y.; Kawachi, S.; Otsu, S.; Tokumaru, K.; Konishi, G. *J. Org. Chem.* **2013**, *78*, 3196–3207.
- (5) Zilbershtein-Shkhanovsky, L.; Weitman, M.; Major, D. T.; Fischer, B. *J. Org. Chem.* **2013**, *78*, 11999–12008.
- (6) Chudakov, D. M.; Matz, M. V.; Lukyanov, S.; Lukyanov, K. A. *Physiol. Rev.* **2010**, *90*, 1103–1163.
- (7) Dedecker, P.; De Schryver, F. C.; Hofkens, J. *J. Am. Chem. Soc.* **2013**, *135*, 2387–2402.
- (8) Ormö, M.; Cubitt, A. B.; Kallio, K.; Gross, L. A.; Tsien, R. Y.; Remington, S. J. *Science* **1996**, *273*, 1392–1395.
- (9) Niwa, H.; Inouye, S.; Hirano, T.; Matsuno, T.; Kojima, S.; Kubota, M.; Ohashi, M.; Tsuji, F. I. *Proc. Natl. Acad. Sci. U. S. A.* **1996**, *93*, 13617–13622.
- (10) Meech, S. R. *Chem. Soc. Rev.* **2009**, *38*, 2922–2934.
- (11) Tolbert, L. M.; Baldrige, A.; Kowalik, J.; Solntsev, K. M. *Acc. Chem. Res.* **2012**, *45*, 171–181.
- (12) Voliani, V.; Bizzarri, R.; Nifosi, R.; Abbruzzetti, S.; Grandi, E.; Viappiani, C.; Beltram, F. *J. Phys. Chem. B* **2008**, *112*, 10714–10722.
- (13) Hsieh, C.-C.; Chou, P.-T.; Shih, C.-W.; Chuang, W.-T.; Chung, M.-W.; Lee, J.; Joo, T. *J. Am. Chem. Soc.* **2011**, *133*, 2932–2943.
- (14) Huang, G.-J.; Cheng, C.-W.; Hsu, H.-Y.; Prabhakar, C.; Lee, Y.-P.; Diau, E. W.-G.; Yang, J.-S. *J. Phys. Chem. B* **2013**, *117*, 2695–2704.
- (15) Park, J. W.; Rhee, Y. M. *J. Am. Chem. Soc.* **2016**, *138*, 13619–13629.
- (16) Wu, L.; Burgess, K. *J. Am. Chem. Soc.* **2008**, *130*, 4089–4096.
- (17) Chuang, W.-T.; Hsieh, C.-C.; Lai, C.-H.; Lai, C.-H.; Shih, C.-W.; Chen, K.-Y.; Hung, W.-Y.; Hsu, Y.-H.; Chou, P.-T. *J. Org. Chem.* **2011**, *76*, 8189–8202.
- (18) Hsu, Y.-H.; Chen, Y.-A.; Tseng, H.-W.; Zhang, Z.; Shen, J.-Y.; Chuang, W.-T.; Lin, T.-C.; Lee, C.-S.; Hung, W.-Y.; Hong, B.-C.; Liu, S.-H.; Chou, P.-T. *J. Am. Chem. Soc.* **2014**, *136*, 11805–11812.
- (19) Baranov, M. S.; Solntsev, K. M.; Baleeva, N. S.; Mishin, A. S.; Lukyanov, S. A.; Lukyanov, K. A.; Yampolsky, I. V. *Chem. - Eur. J.* **2014**, *20*, 13234–13241.
- (20) Yang, J.-S.; Huang, G.-J.; Liu, Y.-H.; Peng, S.-M. *Chem. Commun.* **2008**, 1344–1346.
- (21) Lee, J. S.; Baldrige, A.; Feng, S.; SiQiang, Y.; Kim, Y. K.; Tolbert, L. M.; Chang, Y. T. *ACS Comb. Sci.* **2011**, *13*, 32–38.
- (22) Huang, G.-J.; Ho, J.-H.; Prabhakar, C.; Liu, Y.-H.; Peng, S.-M.; Yang, J.-S. *Org. Lett.* **2012**, *14*, 5034–5037.
- (23) Huang, G.-J.; Lin, C.-J.; Liu, Y.-H.; Peng, S.-M.; Yang, J.-S. *Photochem. Photobiol.* **2015**, *91*, 714–722.
- (24) Gutierrez, S.; Martinez-Lopez, D.; Moron, M.; Sucunza, D.; Sampedro, D.; Domingo, A.; Salgado, A.; Vaquero, J. *J. Chem. - Eur. J.* **2015**, *21*, 18758–18763.
- (25) Deng, H.; Yu, C.; Gong, L.; Zhu, X. *J. Phys. Chem. Lett.* **2016**, *7*, 2935–2944.
- (26) Cheng, C.-W.; Huang, G.-J.; Hsu, H.-Y.; Prabhakar, C.; Lee, Y.-P.; Diau, E. W.-G.; Yang, J.-S. *J. Phys. Chem. B* **2013**, *117*, 2705–2716.
- (27) Chang, D.-H.; Ou, C.-L.; Hsu, H.-Y.; Huang, G.-J.; Kao, C.-Y.; Liu, Y.-H.; Peng, S.-M.; Diau, E. W.-G.; Yang, J.-S. *J. Org. Chem.* **2015**, *80*, 12431–12443.
- (28) Walker, C. L.; Lukyanov, K. A.; Yampolsky, I. V.; Mishin, A. S.; Bommarius, A. S.; Duraj-Thatte, A. M.; Azizi, B.; Tolbert, L. M.; Solntsev, K. M. *Curr. Opin. Chem. Biol.* **2015**, *27*, 64–74.
- (29) Zimmer, M. Non-Retinal Chromophoric Proteins. In *Cis–Trans Isomerization in Biochemistry*; Dugave, C., Eds.; Wiley-VCH: Weinheim, 2006; pp 77–94.
- (30) Hammond, G. S. *J. Am. Chem. Soc.* **1955**, *77*, 334–338.
- (31) Kowalik, J.; Baldrige, A.; Tolbert, L. *Synthesis* **2010**, 2424–2436.
- (32) Baumann, W.; Bischof, H.; Fröhling, J. C.; Brittinger, C.; Rettig, W.; Rotkiewicz, K. *J. Photochem. Photobiol., A* **1992**, *64*, 49–72.
- (33) Yang, J.-S.; Lin, C.-K.; Lahoti, A. M.; Tseng, C.-K.; Liu, Y.-H.; Lee, G.-H.; Peng, S.-M. *J. Phys. Chem. A* **2009**, *113*, 4868–4877.
- (34) Grabowski, Z. R.; Rotkiewicz, K.; Rettig, W. *Chem. Rev.* **2003**, *103*, 3899–4032.
- (35) Baldrige, A.; Samanta, S. R.; Jayaraj, N.; Ramamurthy, V.; Tolbert, L. M. *J. Am. Chem. Soc.* **2010**, *132*, 1498–1499.
- (36) Zhang, G.; Gurtu, V.; Kain, S. R. *Biochem. Biophys. Res. Commun.* **1996**, *227*, 707–711.
- (37) Kremers, G.-J.; Gilbert, S. G.; Cranfill, P. J.; Davidson, M. W.; Piston, D. W. *J. Cell Sci.* **2011**, *124*, 157–160.
- (38) Van, S.-P.; Hammond, G. S. *J. Am. Chem. Soc.* **1978**, *100*, 3895–3902.
- (39) Libralato, G.; Volpi Ghirardini, A.; Avezzu, F. *J. Hazard. Mater.* **2010**, *176*, 535–539.
- (40) Brouwer, A. M. *Pure Appl. Chem.* **2011**, *83*, 2213–2228.
- (41) Yang, J.-S.; Liau, K.-L.; Wang, C.-M.; Hwang, C.-Y. *J. Am. Chem. Soc.* **2004**, *126*, 12325–12335.
- (42) Frisch, M. J.; Trucks, G. W.; Schlegel, H. B.; Scuseria, G. E.; Robb, M. A.; Cheeseman, J. R.; Scalmani, G.; Barone, V.; Mennucci, B.; Petersson, G. A.; Nakatsuji, H.; Caricato, M.; Li, X.; Hratchian, H. P.; Izmaylov, A. F.; Bloino, J.; Zheng, G.; Sonnenberg, J. L.; Hada, M.; Ehara, M.; Toyota, K.; Fukuda, R.; Hasegawa, J.; Ishida, M.; Nakajima, T.; Honda, Y.; Kitao, O.; Nakai, H.; Vreven, T.; Montgomery, J. A., Jr.; Peralta, J. E.; Ogliaro, F.; Bearpark, M.; Heyd, J. J.; Brothers, E.; Kudin, K. N.; Staroverov, V. N.; Kobayashi, R.; Normand, J.; Raghavachari, K.; Rendell, A.; Burant, J. C.; Iyengar, S. S.; Tomasi, J.; Cossi, M.; Rega, N.; Millam, J. M.; Klene, M.; Knox, J. E.; Cross, J. B.; Bakken, V.; Adamo, C.; Jaramillo, J.; Gomperts, R.; Stratmann, R. E.; Yazyev, O.; Austin, A. J.; Cammi, R.; Pomelli, C.; Ochterski, J. W.; Martin, R. L.; Morokuma, K.; Zakrzewski, V. G.; Voth, G. A.; Salvador, P.; Dannenberg, J. J.; Dapprich, S.; Daniels, A. D.; Farkas, O.; Foresman, J. B.; Ortiz, J. V.; Cioslowski, J.; Fox, D. J. *Gaussian 09*; Gaussian, Inc.: Wallingford, CT, 2009.
- (43) Zhao, Y.; Truhlar, D. G. *Theor. Chem. Acc.* **2008**, *120*, 215–241.
- (44) Jacquemin, D.; Perpète, E. A.; Ciofini, I.; Adamo, C.; Valero, R.; Zhao, Y.; Truhlar, D. G. *J. Chem. Theory Comput.* **2010**, *6*, 2071–2085.
- (45) Becke, A. D. *J. Chem. Phys.* **1993**, *98*, 5648–5652.
- (46) Lee, C.; Yang, W.; Parr, R. G. *Phys. Rev. B: Condens. Matter Mater. Phys.* **1988**, *37*, 785–789.
- (47) Rajesh, K.; Somasundaram, M.; Saiganesh, R.; Balasubramanian, K. K. *J. Org. Chem.* **2007**, *72*, 5867–5869.
- (48) Drizin, I.; Altenbach, R.; Carroll, W. Tricyclic dihydropyrazolone and tricyclic dihydroisoxazolone potassium channel openers. U.S. Patent 6,538,004 B2, Mar 25, 2003.